Pharmaceutical Research (2018) 35: 31
https://doi.org/10.1007/s11095-017-2278-0

RESEARCH PAPER

Liposomal Irinotecan Accumulates in Metastatic Lesions, Crosses the Blood-Tumor Barrier (BTB), and Prolongs Survival in an Experimental Model of Brain Metastases of Triple Negative Breast Cancer

Afroz S. Mohammad [1] • Jessica I. Griffith [1] • Chris E. Adkins [1] • Neal Shah [1] • Emily Sechrest [1] • Emma L. Dolan [1] • Tori B. Terrell-Hall [1] • Bart S. Hendriks [2] • Helen Lee [2] • Paul R. Lockman [1]

Received: 18 August 2017 / Accepted: 6 October 2017 / Published online: 9 January 2018

ABSTRACT

Purpose The blood-tumor barrier (BTB) limits irinotecan distribution in tumors of the central nervous system. However, given that the BTB has increased passive permeability we hypothesize that liposomal irinotecan would improve local exposure of irinotecan and its active metabolite SN-38 in brain metastases relative to conventional irinotecan due to enhanced-permeation and retention (EPR) effect.

Methods Female nude mice were intracardially or intracranially implanted with human brain seeking breast cancer cells (brain metastases of breast cancer model). Mice were administered vehicle, non-liposomal irinotecan (50 mg/kg), liposomal irinotecan (10 mg/kg and 50 mg/kg) intravenously starting on day 21. Drug accumulation, tumor burden, and survival were evaluated.

Results Liposomal irinotecan showed prolonged plasma drug exposure with mean residence time (MRT) of 17.7 ± 3.8 h for SN-38, whereas MRT was 3.67 ± 1.2 for non-liposomal irinotecan. Further, liposomal irinotecan accumulated in metastatic lesions and demonstrated prolonged exposure of SN-38 compared to non-liposomal irinotecan. Liposomal irinotecan achieved AUC values of 6883 ± 4149 ng-h/g for SN-38, whereas non-liposomal irinotecan showed significantly lower AUC values of 982 ± 256 ng-h/g for SN-38. Median survival for liposomal irinotecan was 50 days, increased from 37 days ($p<0.05$) for vehicle.

Conclusions Liposomal irinotecan accumulates in brain metastases, acts as depot for sustained release of irinotecan and SN-38, which results in prolonged survival in preclinical model of breast cancer brain metastasis.

KEY WORDS chemotherapy · enhanced permeation and retention · nanoparticles · permeability · pharmacokinetics

ABBREVIATIONS

AUC	Area under the curve
BBB	Blood-brain barrier
BTB	Blood-tumor barrier
Cl	Clearance
CNS	Central nervous system
DAPI	4',6-diamidino-2-phenylindole
DiI5	Carbocyanine tracer DilIC18 (5)-DS
EPR	Enhanced permeation and retention
ER	Estrogen receptor
HER2	Human epidermal growth factor receptor 2
IRN-50	Non-liposomal Irinotecan (50 mg/kg)
MRT	Mean residence time
nal-IRI-10	Nano-liposomal Irinotecan (10 mg/kg, Irinotecan equivalent)
nal-IRI-50	Nano-liposomal (50 mg/kg, Irinotecan equivalent)
P-gp	P-glycoprotein (ABCB1)
PK	Pharmacokinetics
PR	Progesterone receptor
SRS	Stereotaxic radiosurgery
TNBC	Triple negative breast cancer
Vd	Apparent volume of distribution
WBRT	Whole brain radiotherapy

✉ Paul R. Lockman
prlockman@hsc.wvu.edu

[1] School of Pharmacy, Department of Pharmaceutical Sciences, West Virginia University Health Sciences Center, 1 Medical Center Drive, Morgantown, West Virginia 26506-9050, USA

[2] Merrimack Pharmaceuticals, Cambridge, Massachusetts 02139, USA

INTRODUCTION

More than 230,000 women are diagnosed with breast cancer every year (1). Of this general population of women with breast cancer, 6% present with distant metastases at the time of diagnosis, and 10-15% will develop brain metastases at some period during their lifetime. After diagnosis of a brain metastasis, survival is approximately 3-25 months depending on breast cancer subtype, total body burden, and treatment regimen (2,3). Brain metastases are common in human epidermal growth factor receptor 2 overexpressing (HER2+) cancers and triple negative breast cancer (4–6). While the HER2 receptor can be targeted to treat primary breast cancer, unfortunately these therapies (e.g., trastuzumab and lapatinib) have limited distribution to HER2+ brain metastases and accordingly have poor efficacy (6–8). There are no such targeted therapies for the treatment of basal-like triple negative breast cancer (TNBC). Triple negative breast cancer is characterized by the absence of the oncogenic overexpression of HER2, estrogen receptors (ER) and progesterone receptors (PR). Of significance is the fact that brain metastases are a major sequelae of TNBC, as one study found that as many as 36% of women with TNBC will develop metastatic CNS lesions over their lifetime (9).

A major impediment in effectively treating brain metastases of breast cancer is the distribution of chemotherapeutics past the blood-brain barrier (BBB). The BBB, which remains intact to a large degree in metastatic brain lesions of breast cancer (blood-tumor barrier; BTB), significantly limits the passive permeation of drugs from blood to tumor (10,11) and continues to actively extrude and limit lesion accumulation of substrates subject to drug-resistance efflux transporters. For example, paclitaxel, which is used in treating breast cancer, is unable to permeate the BTB at rates to achieve a therapeutically relevant concentration (10,12,13). Approaches to treatment of brain metastases include stereotactic radiosurgery (SRS) or whole brain radiation therapy (WBRT) in combination with systemic therapy, though these therapies are largely palliative and may result in neurocognitive degeneration (14,15).

Nanoparticles and other polymeric drug formulations have shown promise for the delivery of chemotherapeutics, primarily through extravasation across the BTB (11,16,17). This strategy has been particularly effective in fast-growing, aggressive metastases, which produce more growth factors associated with angiogenesis and have a resultant vasculature that is more permeable than BBB (18). In addition, nanoparticles have prolonged residence times within lesions due to increased circulation half-life, while small molecules leave the tumor interstitial space much faster. Consequently, the increased residence time of the nanoparticles results in significantly greater total drug exposure (area under the curve) (19). Improvements in pharmacokinetics and reduced toxicity are evident with nano-liposome encapsulated anticancer agents such as vinorelbine, docetaxel and doxorubicin (20,21).

Recently, Nobel et al. demonstrated that a liposomal nanoparticle increased concentration of irinotecan by 3.1-fold in glioblastoma xenograft tumors compared to non-liposomal irinotecan (22). The 3-fold increase in C_{max} was mirrored by similar increases observed for the active metabolite of irinotecan, SN-38, in the tumor (22). The liposomes preferentially accumulated in tumor tissues, with a 35-fold increase in irinotecan concentration from normal brain concentration, whereas non-liposomal irinotecan showed 9.5 fold increase in irinotecan concentration in tumor tissue compared to normal brain (22). Consistent with previous work showing nanoparticles increase total tumor exposure (area under the curve), the 3.1-fold increased peak concentrations were reached at 12 h in comparison to 15 min with non-liposomal irinotecan (22).

In the clinical setting, delivery of liposomes to brain lesions was previously observed with multiple methods. Detectable and variable uptake of ^{111}In labelled non-PEGylated liposomes at 72 h was observed in brain tumors across multiple patients with malignant glioma using single photon emission tomography(23). In another study, delivery of ^{99m}Tc labelled liposomal doxorubicin to glioblastomas and metastatic brain tumors of various origin was also observed using planar and SPECT scintigraphy (24). Most recently, delivery of ^{64}Cu labelled HER2-targeted liposomal doxorubicin was noted by PET/CT in breast cancer brain metastases (25). These studies highlight the potential for liposomes to enable drug delivery to brain metastases.

We hypothesize that liposomal irinotecan (nal-IRI, irinotecan liposome injection) will effectively deliver irinotecan and SN-38 resulting in efficacy and prolonged survival in a preclinical model of brain metastases of TNBC. nal-IRI, in combination with 5-fluorouracil and leucovorin, has recently been approved in the US and EU for the treatment of patients with advanced metastatic pancreatic adenocarcinoma after disease progression following gemcitabine-based therapy.

MATERIALS AND METHODS

Chemicals

Irinotecan HCl, nal-IRI were supplied by Merrimack Pharmaceuticals (Cambridge, US), which were prepared as reported by Noble et al. and Kalra et al. (22,26). Fluorescently-labeled liposomal irinotecan (DiI5-liposomal irinotecan) was also provided by Merrimack Pharmaceuticals, which was prepared following previously reported methods (27). The lipid mixture of nal-IRI consisting of distearoylphosphatidylcholine, cholesterol, and

polyethyleneglycol-distearoylphosphatidyl-ethanolamine at the molar ration of 3:2:0.015(22). Irinotecan HCl was in the liposomes at a ratio of 750 g irinotecan HCl / mol phospholipid (22). Carbocyanine tracer DiIC18 (5)-DS (D12730; Life Technologies) was incorporated into the lipid bilayer of the liposome prior to drug loading. All other chemicals were analytical grade purchased from Sigma-Aldrich (St. Louis, MO).

Animals

Female athymic nude mice (Charles River Laboratories, Kingston, NY) were used for all experiments in the study. Mice were 6-8 weeks of age and weighed 22-28 g before injecting with cancer cells and were housed under 12-hour light/dark conditions with food and water *ad libitum*, and mice were acclimated for 1 week prior to use. All animal work was approved by West Virginia University Institutional Animal care and Use Committee (IACUC protocols 13-1207). All animal experiments were performed according to the principles of the *Guide for the Care and use of Laboratory animals*.

Cell Culture

Brain-seeking human triple negative breast cancer cells, transfected to express firefly luciferase (MDA-MB-231Br-Luc), were cultured in Dulbecco's Modified Eagle's Medium (DMEM) with 10% fetal bovine serum (FBS). MDA-MB-231Br-Luc cells were kindly provided by Dr. Patricia Steeg, of the National Institute of Health Center for Cancer Research. All cell work was performed under aseptic conditions, and cells were cultured at 37°C with 5% CO_2.

Pharmacokinetic Study of Irinotecan and Liposomal Irinotecan in Brain Tumors

MDA-MB-231Br-Luc cells (5×10^5) cells were injected intracranially as described previously (28). Tumors were allowed to grow until neurological symptoms developed, and the animals were intravenously administered Non-liposomal irinotecan (50 mg/kg, IRN-50), and two different doses of liposomal irinotecan, 10 mg/kg (nal-IRI-10) and 50 mg/kg (nal-IRI-50). Non-liposomal irinotecan-treated animals (n=5/time point) were sacrificed at 0.083, 0.5, 1, 2, 6, 12 and 24 h after administration, and liposomal irinotecan treated animals (n=5/time point) were sacrificed at 0.5, 2, 6, 24, 72, 48 and 168 h after administration. The animals were anesthetized (ketamine/xylazine; 100 mg/kg and 8 mg/kg respectively) and sacrificed by decapitation to collect blood, tumor, and normal brain tissue samples. Irinotecan and SN-38 concentrations in normal brain and brain tumor samples were analyzed by liquid chromatography-tandem mass spectrometry (LC/MS) at Roswell Park Cancer Institute's Bioanalytics, Metabolomics & Pharmacokinetics (BMPK) Facility. Metabolite levels in plasma samples were measured using high performance liquid chromatography (HPLC) methods reported previously (26). The limit of quantification for irinotecan was 25 ng/ml and for its active metabolite SN-38 was 2 ng/ml. A non-compartmental analysis was used to study plasma pharmacokinetic parameters for irinotecan and its active metabolite SN-38 from liposomal formulation and compared to non-liposomal formulation The calculated parameters include area under the curve (AUC) and area under the first moment curve (AUMC) using linear trapezoid method; mean residence time (MRT), where MRT = AUMC/AUC; clearance (Cl), where Cl= Dose/AUC; volume of distribution (Vd), where Vd= MRT × Cl. The data are presented as mean ± SD.

Survival of Animals with Brain Metastases After Treatment

MDA-MB-231Br-Luc cells (1.75×10^5) cells were injected intracardially into the left ventricle and allowed to develop into CNS metastases for 21 days. The presence of metastases was confirmed by bioluminescence imaging (BLI) using the IVIS Lumina *in vivo* imaging system (PerkinElmer, Waltham, MA) after 15 min intraperitoneal administration of D-luciferin potassium salt (150 mg/kg; PerkinElmer). Animals were then randomized into treatment groups (Saline, n=10), IRN-50 (n=10), nal-IRI-10 (n=10), and nal-IRI-50 (n=10). Drugs were administered intravenously via tail vein injection. Treatments were repeated once weekly, and BLI data was gathered twice weekly to quantify tumor burden and progression in different groups, similar to our previous work (16). Once animals developed neurological symptoms, they were sacrificed under anesthesia.

Uptake and Accumulation of Liposomal Irinotecan Formulation

Animals from the liposomal irinotecan group were administered with Dil5-labelled liposomes intravenously. After 24 h, animals were sacrificed under anesthesia as described above. The brain was immediately harvested, frozen in 2-methylbutane at -50°C, and sectioned into 20 μm thick sections (Leica CM3050 S cryostat). The sections were imaged with an Olympus MVX10 microscope with a 2x objective (NA=0.5) using the Cy5 channel. The same sections were then stained with cresyl violet and compared to fluorescent images to confirm the accumulation of Dil-5 labeled liposomes within the metastatic tumors. Sections were also stained for cytokeratin and DAPI, a fluorescent stain that binds to DNA to visualize the accumulation of liposomes within the cancer cell using Nikon N-Storm super-resolution microscope system.

Data Analysis

Differences among treatment groups in the survival study were compared by log-rank test (GraphPad® Prism 6.0, San Diego, CA) and were considered statistically significant at $p<0.05$. Living Image V4.0 software (PerkinElmer, Waltham, MA) was used to quantify tumor burden in different groups.

RESULTS

Liposomal Irinotecan Increased Plasma Half-Life and Total Exposure of Both Irinotecan and its Active Metabolite SN-38

Initially, we set out to study the plasma concentration time profile of irinotecan and its active metabolite, SN-38, after the administration of IRN-50, nal-IRI-10, and nal-IRI-50. We observed the plasma half-life of irinotecan increased in liposomal formulations, nal-IRI-10 and nal-IRI-50 with half-lives of 12.7 ± 0. 5 h and 10.9 ± 0.3 h respectively, when compared to that of IRN-50 with a half-life of 3.3 ± 0.1 h. Plasma half-life of SN-38 was also increased for nal-IRI with 21 ± 2.9 h in nal-IRI-10 group and 18 ± 1.3 h in nal-IRI-50 group when compared to that of IRN-50 with a half-life of 3.17 ± 0.43 h (Table I). We also observed that the mean residence time (MRT) for liposomal formulation increased with 4.5 ± 0.4 h for nal-IRI-10 and 7.3 ± 2.6 h for nal-IRI-50, whereas IRI-50 showed MRT of 2 ± 0.5 h for plasma irinotecan. We found similar trend for its active metabolite SN-38 with MRT of 16.7 ± 8.3 h and 17.7 ± 3.8 h for nal-IRI-10 and nal-IRI-50 respectively, while MRT for IRI-50 was 3.67 ± 1.2 (Table I). Clearance (Cl) of irinotecan for IRI-50 was 85.7 ± 22.8 ml/h with apparent volume of distribution (Vd) 178.6 ± 64.7, whereas for liposomal irinotecan clearance and volume of distribution significantly decreased with values 0.6 ± 0.2 ml/h and 2.9 ± 0.5 ml respectively for nal-IRI-10 and clearance value of 0.3 ± 0.1 ml/h and volume of distribution of 2.2 ± 1.1 ml for nal-IRI-50. We have seen the similar trend for plasma SN-38 clearance and volume of distribution values, for liposomal irinotecan both clearance and volume of distribution values were significantly lower than that of IRI-150 values (Table I).

We also observed the area under the curve (AUC) significantly increased with nal-IRI, 3.20± 0.94 ng-hr/ml $\times 10^5$ for nal-IRI-10 and 45.05 ± 5.52 ng-hr/ml $\times 10^5$ for nal-IRI-50 compared with IRN-50, which had an AUC of 0.15 ± 0.02 ng-hr/ml $\times 10^5$ (Fig. 1b). With the increase in AUC for free irinotecan from nal-IRI formulations, we also observed significant increase in AUC for the active metabolite SN-38 from the liposomal formulations with 2.56 ±0.63 ng-hr/ml $\times 10^3$ for nal-IRI-10 and 9.66 ± 0.44 ng-hr/ml $\times 10^3$ for nal-IRI-50, compared to the AUC for IRN-50 at 0.55 ± 0.08 ng-hr/ml $\times 10^3$ (Fig. 1d). These results confirm the increased plasma exposure of irinotecan and its active metabolite SN-38 from nal-IRI-10 and nal-IRI-50 formulations when compared to IRN-50 (Fig. 1).

Dil-5 Labelled Liposomes Cross the BTB and Accumulate in Brain Metastases

To understand tumor localization of nal-IRI, we studied the spatial distribution of the liposomal formulation incorporated with a fluorescent dye (Dil-5). After confirmation of the presence of metastatic lesions by BLI (Fig. 2a), Dil5-labelled liposomes were administered and allowed to circulate for 24 hr, at which time brain tissue was harvested and sectioned to allow for microscopic distribution visualization (Fig. 2b). Brain sections corresponding to regions 1, 2, 3 and 4, as shown in Fig. 2b, were also imaged for visualization of Dil-5 liposomes (Fig. 2D1-D4). The same sections were stained with cresyl violet and imaged for histopathologic visualization of lesions (Fig. 2 C1-C4). Cresyl violet images (Fig. 2 C1-C4) and their corresponding fluorescent images (Fig. 2 D1-D4) show that there is localization of Dil-5 liposomes within metastatic

Table I Plasma Pharmacokinetics of Non-Liposomal Irinotecan and Liposomal Irinotecan

Treatment	$AUC_{0-\alpha}$ (ng-hr/mL) $\times 10^5$	$t_{1/2}$ (h)	MRT (h)	Cl (ml/h)	Vd (ml)
Plasma Irinotecan					
IRI-50	0.2 ± 0.02	3.3 ± 0.1	2 ± 0.5	85.7 ± 22.8	178.6 ± 64.7
nal-IRI-10	3.2± 0.9	12.7 ± 0.5	4.5 ± 0.4	0.6 ± 0.2	2.9 ± 0.5
nal-IRI-50	45 ± 5.5	10.9 ± 0.3	7.3 ± 2.6	0.3 ± 0.1	2.2 ± 1.1
Treatment	$AUC_{0-\alpha}$ (ng-hr/mL) $\times 10^3$	$t_{1/2}$ (h)	MRT (h)	Cl (ml/h)	Vd (ml)
Plasma SN-38					
IRI-50	0.6 ± 0.08	4.32 ± 3.2	3.67 ± 1.2	2472 ± 881	7845.6 ± 2023
nal-IRI-10	2.6 ±0.6	21 ± 2.9	16.7 ± 8.3	80.9 ± 13.5	1327.5 ± 678
nal-IRI-50	9.7 ± 0.4	18 ± 1.3	17.7 ± 3.8	130.2 ±11.9	1990.3 ± 329

$AUC_{0-\alpha}$ Area under the time-concentration cure, *Cl* Clearance, *MRT* Mean residence time, *$t_{1/2}$* plasma half-life of the drug, *Vd* Apparent volume of distribution

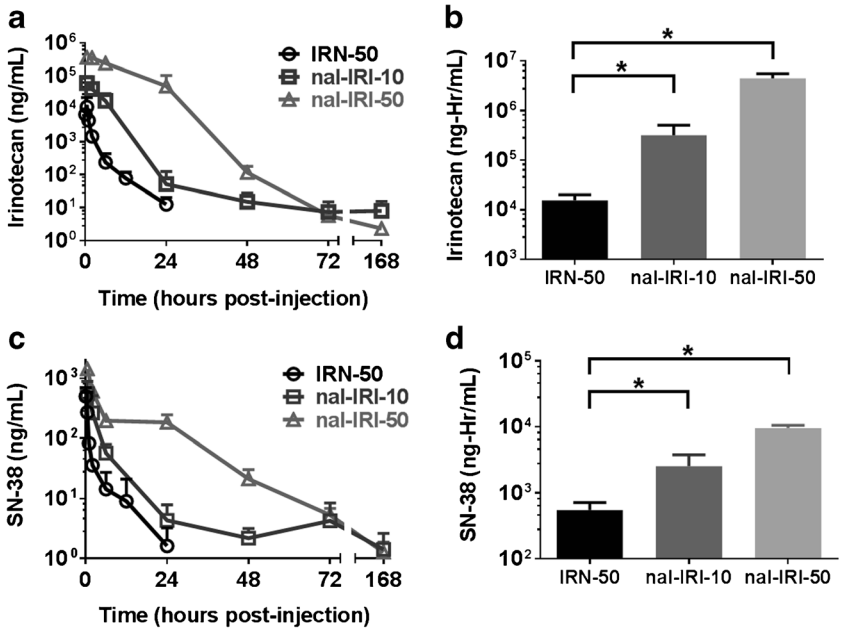

Fig. 1 (**a** and **c**) Plasma concentration-time profile of irinotecan and its active metabolite SN-38 after IV bolus administration of IRN-50, nal-IRI-10 and nal-IRI -50. Irinotecan and SN-38 essentially cleared from circulation within 24 hr from IRN-50, whereas in nal-IRI-10 and nal-IRI -50 formulations, we observed a prolonged exposure of both irinotecan and SN-38 until 168 hr. (**b** and **d)** Plasma drug exposure of irinotecan and SN-38 expressed by area under the curve (AUC) after IV bolus administration of IRN-50, nal-IRI -10 and nal-IRI -50. Both Irinotecan and SN-38 AUCs for nal-IRI -10 and nal-IRI -50 were significantly higher than that of IRN-50 ($p<0.05$). Data represents mean ± SD for n=4 animals per time point.

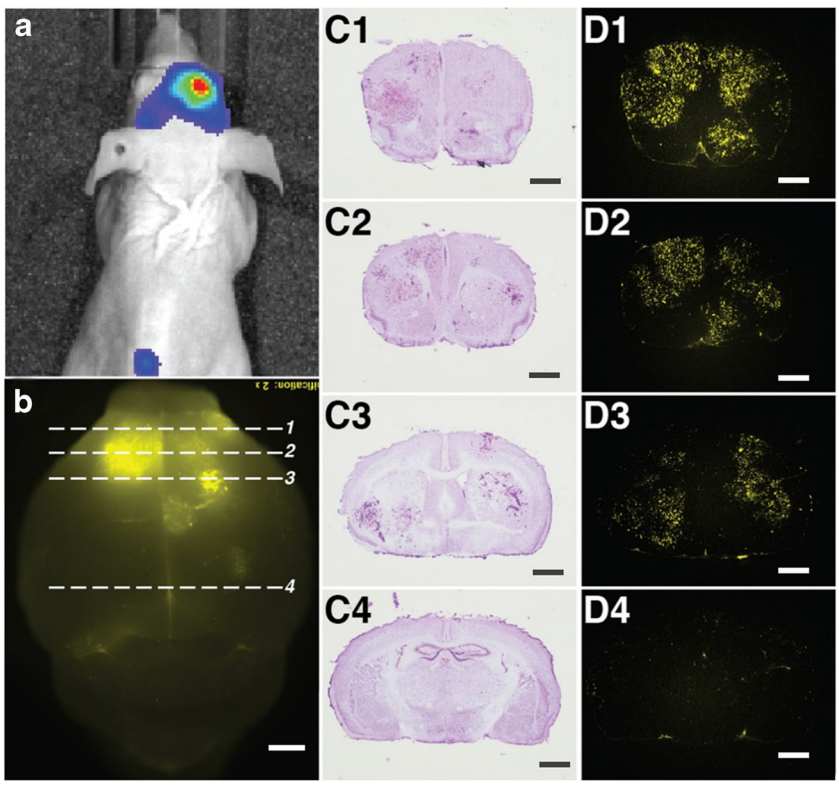

Fig. 2 DiI5-labelled liposomes accumulates in metastatic lesions in preclinical brain metastases of breast cancer model after 24 hr intravenous administration. (**a**) Image showing MDA-MB-231Br-Luc brain metastases BLI signal before administration of DiI5-labelled liposomes. (**b**) Image showing accumulation of fluorescent liposomes in brain after 24 hr circulation. The numbered dashed lines 1, 2, 3 and 4 corresponds to the numbered coronal sections (C and D panels). (**c**) Brain metastases localization and identification of coronal sections based on cresyl violet staining. (C1 = Bregma 2.24 mm; C2=1.54 mm; C3= 0.5 mm; C4= -0.7 mm). (**d**) DiI5 Florescence shows the accumulation of liposomes in the corresponding brain tumors. (D1 = Bregma 2.24 mm; D2=1.54 mm; D3= 0.5 mm; D4= -0.7 mm). Scale bars = 1 mm.

lesions (i.e. cresyl violet positive regions). We also confirmed normal brain tissue (i.e. brain regions devoid of any metastases) has undetectable amounts of Dil-5 labelled liposomes (Fig. 2 C4 and 2D4). The sections were then stained for cytokeratin and DAPI for high-resolution visualization within the metastatic lesions using Nikon N-Storm super-resolution microscope system (Fig. 3). We found that the Dil5 labelled liposomes not only crossed the BTB, but also localized within the cancer cells in the perinuclear regions, as shown in Fig. 3.

Liposomal Irinotecan Acts as Reservoir and Increase the Exposure of Irinotecan and SN-38 in Brain Tumors

After confirming preferential accumulation of Dil-5 labelled liposomes in brain tumors, we set out to assess the concentrations of irinotecan, and its active metabolite, SN-38, in metastatic lesions and normal brain tissue after the administration of liposomal formulations and conventional irinotecan. After the administration of IRN-50, irinotecan and SN-38 concentrations in brain tumors peaked at 0.5 to 2 h post-administration (Fig. 4a and c). Both irinotecan and SN-38 were cleared rapidly after 6 h with tumor-to-plasma ratios ranged from 3.0 to 10 for irinotecan and 0.62-5.1 for SN-38 (Fig 4a and c). After administration of nal-IRI-50, irinotecan and SN-38 concentrations continue to accumulate in brain tumors over 168 h with tumor-to-plasma ratios of 0.05-90 and 0.59-39 for irinotecan and SN-38, respectively. Tumor SN-38 concentration in mice treated with nal-IRI-50 at 168 h was found to be 50 ± 30 ng/g, whereas SN-38 concentration in non-liposomal irinotecan treated group was undetectable (<10 ng/g) at 12 h post-administration (Fig. 4c). The AUC of both irinotecan and SN-38 from nal-IRI-50 in brain tumors was found to be significantly higher than that of IRN-50 (Fig. 4b and d). These results suggest that nal-IRI prolonged drug exposure in brain tumors compared to conventional irinotecan.

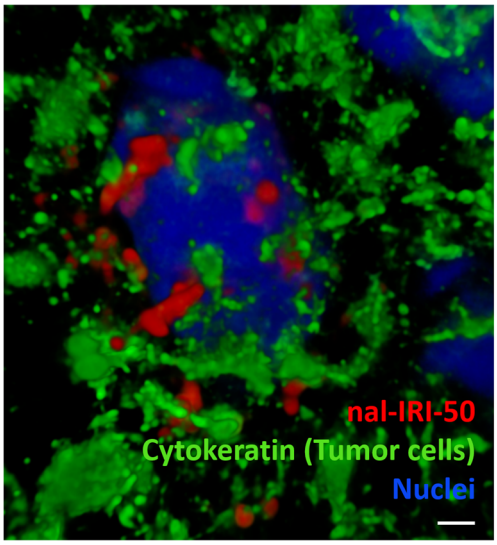

Fig. 3 Dil5-labelled liposomes accumulate in metastatic lesions in preclinical brain metastases of breast cancer model 24 hr after intravenous administration. Mouse brain tissue sections were stained for DAPI (blue) and cytokeratin (green) after 24 hr circulation of Dil5-labelled liposomes. DAPI highlights the nucleus and cytokeratin highlights MDA-MB-231Br-Luc brain metastases. We observed Dil5-labelled liposomes (red) accumulated in the MDA-MB-231Br-Luc cancer cell (green) around the nucleus (blue). Images were acquired from Nikon N-Storm super-resolution microscope system. Scale bar = 1 μm.

Liposomal Irinotecan Reduces Tumor Burden and Prolongs Survival in Animals with Brain Metastases of Breast Cancer

Lastly, we set out to determine if the increased accumulation of Dil5-liposomal irinotecan and prolonged drug exposure would result in increased median survival in our experimental model. To evaluate this, mice injected with TNBC cells intracardially for metastases development; after 21 days, mice were randomized to receive different therapeutic treatment regimens (Saline, IRN-50, nal-IRI-10 and nal-IRI-50). We observed that progression of tumor burden in liposomal irinotecan-treated groups (nal-IRI-10 and nal-IRI-50) was significantly lowered when compared to vehicle and IRN-50 groups (Fig. 5a and b). We also noted that liposomal irinotecan formulations significantly improved survival when compared to both the vehicle group and conventional irinotecan group (Fig. 6). The median survival for liposomal irinotecan groups were 48 and 50 days for nal-IRI-10 and nal-IRI-50 respectively, while for vehicle and non-liposomal irinotecan (50 mg/kg) group's median survival were 37 and 35 days, respectively (Fig.6).

DISCUSSION

The results of this study show that nal-IRI penetrates the BTB and accumulates within metastases in a preclinical model of MDA-MB-231Br-Luc brain metastases. Upon accumulation in metastatic tumors, the liposomes appear to act as reservoir for the release of irinotecan. The local release of irinotecan improved free drug exposure to tumor and presumably delayed the progression of tumor burden, which ultimately corresponded to significant prolonged survival.

In general, nanoparticles with sizes ranging from 80 to 200 nm are expected to have optimal tumor distribution and accumulation due to enhanced permeation and retention (EPR) through the leaky vasculature of tumors (18,29,30). It has been posited, based upon liver and renal clearance of nanoparticles, that ideal size of liposomes for maximum distribution and to maintain prolonged plasma residence times is approximately 100 nm (31). The liposomal irinotecan formulation described in this study were between 100-110 nm (22). Once liposomes accumulate in tumors due to EPR effect, the

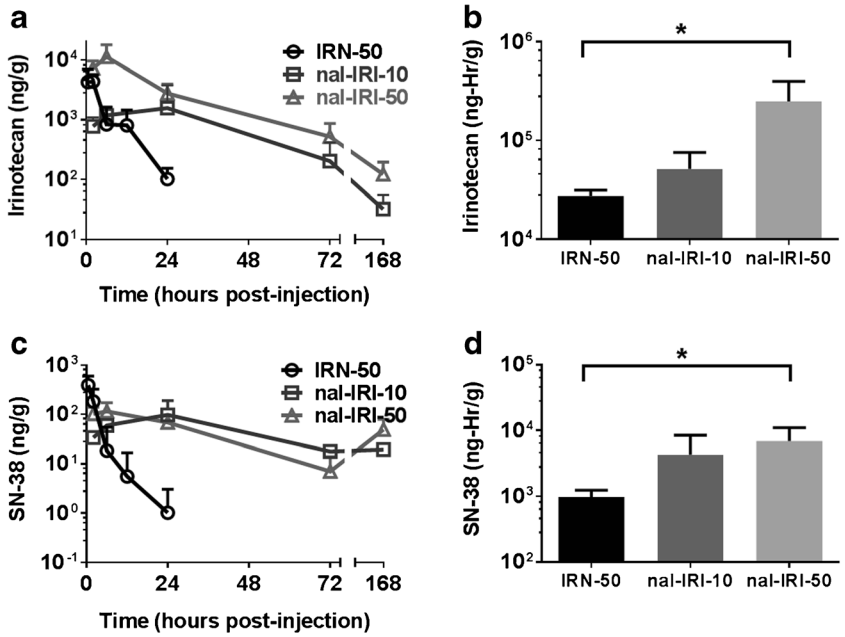

Fig. 4 (**a** and **c**) Brain tumor concentration-time profiles of irinotecan and active metabolite SN-38 after IV bolus administration of IRN-50, nal-IRI -10 and nal-IRI -50. Irinotecan and SN-38 nearly cleared from circulation within 24 hr from IRN-50, whereas in nal-IRI -10 and nal-IRI -50 formulations, we observed a prolonged exposure of both irinotecan and SN-38 until 168 hr. (**b** and **d**) Brain tumor exposure of irinotecan and SN-38 expressed by area under the curve (AUC) after IV bolus administration of IRN-50, nal-IRI -10 and nal-IRI -50. Both Irinotecan and SN-38 AUCs for nal-IRI -50 were significantly higher than that of IRN-50 ($p<0.05$). Data represents mean ± SD for n=4 animals per time point.

clearance from the tumor is limited because of its size and impaired lymphatic system, which results in prolonged drug exposure (32,33). On the other hand, non-liposomal irinotecan is rapidly cleared from the tumor due to its smaller size, leading to sub-therapeutic drug levels in tumor between the cycles of treatment. The accumulation of Dil-5 labelled liposomes in brain metastases, and the increased concentrations of drug payload over a period of time align with previous observations of passive targeting in tumors with nanoparticles like liposomes (34,35). These observations support that liposomal irinotecan

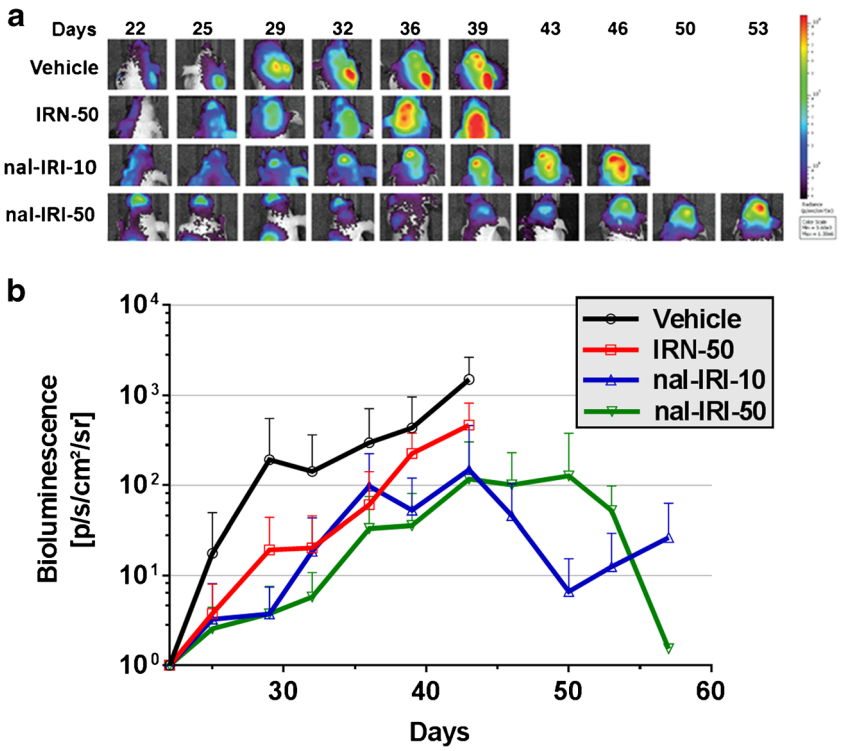

Fig. 5 (**a**) *In vivo* optical imagining (IVIS Lumina) was used to confirm and monitor the metastatic tumor growth after intracardiac injection. Increase in BLI signal in brain reflects the pattern of metastatic tumor growth in different treatment groups. Images acquired are of same animal sequentially over time. (**b**) Mean BLI signal *versus* time in mice exhibiting brain metastases. Treatment was initiated on day 21. Each data point represents mean ± SD. Tumor burden in groups treated with liposomal irinotecan were significantly lower ($P<0.05$).

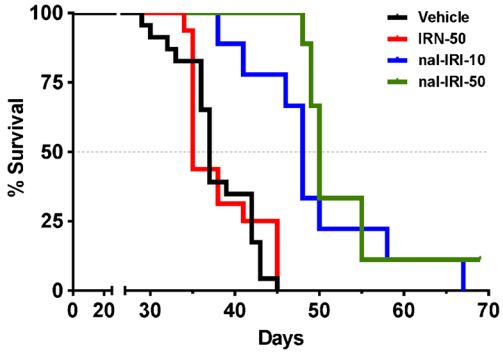

Fig. 6 Kaplan-Meier Survival Plot of mice bearing metastatic brain tumors from human triple negative breast cancer. The mice were treated weekly via IV bolus with vehicle (n=23), IRN-50 (n = 16), nal-IRI -10 (n=8) and nal-IRI -50 (n=9) starting 21 days after intracardiac injection of MDA-MB-231Br-Luc cancer cells. The median survival time was 37 days for vehicle, 35 days for IRN-50, 48 and 50 days for nal-IRI -10 and nal-IRI -50 respectively. The median survival for liposomal irinotecan groups (nal-IRI -10 and nal-IRI -50) significantly increased ($P < 0.05$) when compared to vehicle group. The groups were compared to vehicle by Log-rank statistical analysis.

accumulates in brain metastases via the EPR effect, similar to that reported for other solid tumor types (26). This maintenance of prolonged SN-38 cytotoxic concentrations and high tumor-to-normal tissue ratio are likely responsible for the prolonged survival observed in our animal model.

Further mechanistic possibilities for the increased drug uptake and accumulation from liposomal irinotecan is that it may avoid efflux by multidrug resistant proteins like P-gp and BCRP (12,36–38). The uptake of conventional anticancer agents is limited by multidrug resistant protein present on membranes of cancer cells (38). In addition to efflux mechanisms on cancer cells, the BBB and BTB also express variety of multidrug resistant proteins, which further limits the uptake of chemotherapy (39). Uptake of conventional irinotecan is also restricted by P-gp efflux (12,38,40), but we hypothesize that the liposomal irinotecan formulation bypasses multidrug resistant proteins both at the BBB/BTB and the efflux proteins associated with cancer cells (41,42).

Irinotecan is a widely used chemotherapeutic agent, upon administration it is converted to its active metabolite SN-38, which is a potent topoisomerase I inhibitor (16). Irinotecan is mostly converted to SN-38 in liver, whereas, liposomal irinotecan formulation leads to local conversion of irinotecan to SN-38 upon accumulation in the tumor (43). We observed that clearance rates for both irinotecan and its active metabolite SN-38 was significantly lower in liposomal irinotecan groups when compared to non-liposomal irinotecan group and this lower clearance rates for liposomes are responsible for prolonged plasma halves and mean residence times for both irinotecan and SN-38 with liposomal irinotecan formulation. The rate of clearance for liposomes are determined by both drug release and also uptake of liposomes by mononuclear phagocyte system (MPS) (44,45). The liposomes used for this study are "PEGylated" with approximately one polyethyleneglycol (PEG) molecule for 200 phospholipid molecules and PEGylated liposomes have long circulation time (46,47). This increase in circulation time also accounts for the decrease in volume of distribution of both irinotecan and SN-38 from liposomal formulations when compared to non-liposomal irinotecan formulation (Table I).

In addition to preferential accumulation of liposomal irinotecan in metastatic lesions, we observed that the progression of tumor burden was delayed in liposomal irinotecan groups, which correlated with prolonged survival. The median survival of the vehicle group was found to be 37 days (16,48). Treatment with conventional irinotecan (50 mg/kg) showed no improvement in survival (median survival of 35 days). However, liposomal irinotecan-treated groups significantly prolonged median survival to 50 days in 50 mg/kg group and 48 days in 10 mg/kg group (Fig.6). We hypothesize that after accumulation of liposomal irinotecan formulation in brain tumors, they act as reservoir for the release of irinotecan as described in other previous studies (49,50). The prolonged release of the chemotherapy from the liposomes provides sustained tumor drug concentration, as shown in the pharmacokinetic results. Maintenance of the irinotecan concentration in between cycles of treatments in liposomal irinotecan groups may be responsible for the prolonged survival when compared to vehicle and conventional irinotecan groups. We have demonstrated that nal-IRI permeates the BTB and accumulates in metastatic brain tumors due to the EPR effect, prolonged systemic circulation, and potentially bypassing the efflux mechanisms. We also observed accumulation of liposomes in lesions with sustained release of irinotecan. We believe this is responsible for the increase in survival in liposomal irinotecan groups compared to non-liposomal irinotecan group. Clinically, the chemotherapy used for the management of brain metastases of breast cancer are conventional cytotoxic agents such as cyclophosphamide, fluorouracil, methotrexate, and doxorubicin based upon their increased permeability through tumor vasculature (51,52). Collectively, results presented herein support the on-going clinical study of nal-IRI in patients with breast cancer brain metastases (NCT01770353) and indicates its potential for treatment of brain metastases of breast cancer.

CONCLUSIONS

In summary, we demonstrated efficacy of liposomal irinotecan in a preclinical model of a metastatic brain tumors. We observed the preferential uptake and accumulation of liposomal irinotecan into the brain tumors, followed by sustained concentration of irinotecan and its active metabolite SN-38 in plasma and tumor, ultimately correlating with increased survival.

ACKNOWLEDGMENTS AND DISCLOSURES. This research was supported by Merrimack Pharmaceuticals, Inc., and a grant from the National Cancer Institute (R01CA166067-01A1). Publication support was received from Ipsen Biopharmaceuticals, Inc. Additional support for this research was provided through the National Institute of General Medical Sciences of the National Institutes of Health (CTSI Award: U54GM104942, and the CoBRE P30 GM103488).

REFERENCES

1. Society AC. Breast cancer facts & figures 2015–2016. 2015.
2. Sperduto PW, Kased N, Roberge D, Xu Z, Shanley R, Luo X, et al. Summary report on the graded prognostic assessment: an accurate and facile diagnosis-specific tool to estimate survival for patients with brain metastases. J Clin Oncol. 2012;30(4):419–25.
3. Siegel RL, Miller KD, Jemal A. Cancer statistics, 2015. CA Cancer J Clin. 2015;65(1):5–29.
4. H. Nitta BD Kelly, C. Alfred, S. Jewell, P. Banks, E. Dennis, T.M. Grogan. The assessment of HER2 status in breast cancer: the past, the present, and the future. Pathol Int. 2016.
5. Bachelot T, Romieu G, Campone M, Dieras V, Cropet C, Dalenc F, et al. Lapatinib plus capecitabine in patients with previously untreated brain metastases from HER2-positive metastatic breast cancer (LANDSCAPE): a single-group phase 2 study. Lancet Oncol. 2013;14(1):64–71.
6. Bohn KA, Adkins CE, Mittapalli RK, Terrell-Hall TB, Mohammad AS, Shah N, et al. Semi-automated rapid quantification of brain vessel density utilizing fluorescent microscopy. J Neurosci Methods. 2016.
7. Morikawa A, Peereboom DM, Thorsheim HR, Samala R, Balyan R, Murphy CG, et al. Capecitabine and lapatinib uptake in surgically resected brain metastases from metastatic breast cancer patients: a prospective study. Neuro-Oncology. 2015;17(2):289–95.
8. Taskar KS, Rudraraju V, Mittapalli RK, Samala R, Thorsheim HR, Lockman J, et al. Lapatinib distribution in HER2 overexpressing experimental brain metastases of breast cancer. Pharm Res. 2012;29(3):770–81.
9. Lin NU, Vanderplas A, Hughes ME, Theriault RL, Edge SB, Wong YN, et al. Clinicopathologic features, patterns of recurrence, and survival among women with triple-negative breast cancer in the National Comprehensive Cancer Network. Cancer. 2012;118(22):5463–72.
10. Lockman PR, Mittapalli RK, Taskar KS, Rudraraju V, Gril B, Bohn KA, et al. Heterogeneous blood-tumor barrier permeability determines drug efficacy in experimental brain metastases of breast cancer. Clin Cancer Res Off J Am Assoc Cancer Res. 2010;16(23):5664–78.
11. Mittapalli RK, Adkins CE, Bohn KA, Mohammad AS, Lockman JA, Lockman PR. Quantitative fluorescence microscopy measures vascular pore size in primary and metastatic brain tumors. Cancer Res. 2017;77(2):238–46.
12. Adkins CE, Mittapalli RK, Manda VK, Nounou MI, Mohammad AS, Terrell TB, et al. P-glycoprotein mediated efflux limits substrate and drug uptake in a preclinical brain metastases of breast cancer model. Front Pharmacol. 2013;4:136.
13. Geldenhuys WJ, Mohammad AS, Adkins CE, Lockman PR. Molecular determinants of blood-brain barrier permeation. Ther Deliv. 2015;6(8):961–71.
14. Halasz LM, Uno H, Hughes M, D'Amico T, Dexter EU, Edge SB, et al. Comparative effectiveness of stereotactic radiosurgery versus whole-brain radiation therapy for patients with brain metastases from breast or non-small cell lung cancer. Cancer. 2016;122(13):2091–100.
15. El-Habashy SE, Nazief AM, Adkins CE, Wen MM, El-Kamel AH, Hamdan AM, et al. Novel treatment strategies for brain tumors and metastases. Pharm Pat Anal. 2014;3(3):279–96.
16. Adkins CE, Nounou MI, Hye T, Mohammad AS, Terrell-Hall T, Mohan NK, et al. NKTR-102 Efficacy versus irinotecan in a mouse model of brain metastases of breast cancer. BMC Cancer. 2015;15:685.
17. Mittapalli RK, Liu X, Adkins CE, Nounou MI, Bohn KA, Terrell TB, et al. Paclitaxel-hyaluronic nanoconjugates prolong overall survival in a preclinical brain metastases of breast cancer model. Mol Cancer Ther. 2013;12(11):2389–99.
18. Greish K. Enhanced permeability and retention (EPR) effect for anticancer nanomedicine drug targeting. Methods Mol Biol. 2010;624:25–37.
19. Sambade M, Deal A, Schorzman A, Luft JC, Bowerman C, Chu K, et al. Efficacy and pharmacokinetics of a modified acid-labile docetaxel-PRINT((R)) nanoparticle formulation against non-small-cell lung cancer brain metastases. Nanomedicine (Lond). 2016;11(15):1947–55.
20. Drummond DC, Noble CO, Guo Z, Hayes ME, Park JW, Ou CJ, et al. Improved pharmacokinetics and efficacy of a highly stable nanoliposomal vinorelbine. J Pharmacol Exp Ther. 2009;328(1):321–30.
21. Maeda H, Nakamura H, Fang J. The EPR effect for macromolecular drug delivery to solid tumors: Improvement of tumor uptake, lowering of systemic toxicity, and distinct tumor imaging in vivo. Adv Drug Deliv Rev. 2013;65(1):71–9.
22. Noble CO, Krauze MT, Drummond DC, Forsayeth J, Hayes ME, Beyer J, et al. Pharmacokinetics, tumor accumulation and antitumor activity of nanoliposomal irinotecan following systemic treatment of intracranial tumors. Nanomedicine (Lond). 2014;9(14):2099–108.
23. Khalifa A, Dodds D, Rampling R, Paterson J, Murray T. Liposomal distribution in malignant glioma: possibilities for therapy. Nucl Med Commun. 1997;18(1):17–23.
24. Koukourakis MI, Koukouraki S, Fezoulidis I, Kelekis N, Kyrias G, Archimandritis S, et al. High intratumoural accumulation of stealth liposomal doxorubicin (Caelyx) in glioblastomas and in metastatic brain tumours. Br J Cancer. 2000;83(10):1281–6.
25. Lee H, Shields AF, Siegel BA, Miller KD, Krop I, Ma CX, et al. 64Cu-MM-302 positron emission tomography quantifies variability of enhanced permeability and retention of nanoparticles in relation to treatment response in patients with metastatic breast cancer. Clin Cancer Res Off J Am Assoc Cancer Res. 2017.
26. Kalra AV, Kim J, Klinz SG, Paz N, Cain J, Drummond DC, et al. Preclinical activity of nanoliposomal irinotecan is governed by tumor deposition and intratumor prodrug conversion. Cancer Res. 2014;74(23):7003–13.
27. Espelin CW, Leonard SC, Geretti E, Wickham TJ, Hendriks BS. Dual HER2 targeting with trastuzumab and liposomal-encapsulated doxorubicin (MM-302) demonstrates synergistic antitumor activity in breast and gastric cancer. Cancer Res. 2016;76(6):1517–27.
28. Adkins CE, Nounou MI, Mittapalli RK, Terrell-Hall TB, Mohammad AS, Jagannathan R, et al. A novel preclinical method to quantitatively evaluate early-stage metastatic events at the murine blood–brain barrier. Cancer Prev Res. 2015;8(1):68–76.
29. Yuan F, Dellian M, Fukumura D, Leunig M, Berk DA, Torchilin VP, et al. Vascular permeability in a human tumor xenograft: molecular size dependence and cutoff size. Cancer Res. 1995;55(17):3752–6.

30. Raza K, Shareef MA, Singal P, Sharma G, Negi P, Katare OP. Lipid-based capsaicin-loaded nano-colloidal biocompatible topical carriers with enhanced analgesic potential and decreased dermal irritation. J Liposome Res. 2014;24(4):290–6.
31. Drummond DC, Meyer O, Hong K, Kirpotin DB, Papahadjopoulos D. Optimizing liposomes for delivery of chemotherapeutic agents to solid tumors. Pharmacol Rev. 1999;51(4):691–743.
32. Iwai K, Maeda H, Konno T. Use of oily contrast medium for selective drug targeting to tumor: enhanced therapeutic effect and X-ray image. Cancer Res. 1984;44(5):2115–21.
33. Abrams HL. The response of neoplastic renal vessels to epinephrine in man. Radiology. 1964;82:217–24.
34. Jain RK, Stylianopoulos T. Delivering nanomedicine to solid tumors. Nat Rev Clin Oncol. 2010;7(11):653–64.
35. Liu J, Yu M, Zhou C, Yang S, Ning X, Zheng J. Passive tumor targeting of renal-clearable luminescent gold nanoparticles: long tumor retention and fast normal tissue clearance. J Am Chem Soc. 2013;135(13):4978–81.
36. Michieli M, Damiani D, Ermacora A, Masolini P, Michelutti A, Michelutti T, et al. Liposome-encapsulated daunorubicin for PGP-related multidrug resistance. Br J Haematol. 1999;106(1):92–9.
37. Lo YL, Tu WC. Co-encapsulation of chrysophsin-1 and epirubicin in PEGylated liposomes circumvents multidrug resistance in HeLa cells. Chem Biol Interact. 2015;242:13–23.
38. Bansal T, Mishra G, Jaggi M, Khar RK, Talegaonkar S. Effect of P-glycoprotein inhibitor, verapamil, on oral bioavailability and pharmacokinetics of irinotecan in rats. Eur J Pharm Sci Off J Eur Fed Pharm Sci. 2009;36(4-5):580–90.
39. Mittapalli RK, Chung AH, Parrish KE, Crabtree D, Halvorson KG, Hu G, et al. ABCG2 and ABCB1 limit the efficacy of dasatinib in a PDGF-B-driven brainstem glioma model. Mol Cancer Ther. 2016;15(5):819–29.
40. Mittapalli RK, Manda VK, Bohn KA, Adkins CE, Lockman PR. Quantitative fluorescence microscopy provides high resolution imaging of passive diffusion and P-gp mediated efflux at the in vivo blood-brain barrier. J Neurosci Methods. 2013;219(1):188–95.
41. Ma P, Mumper RJ. Anthracycline nano-delivery systems to overcome multiple drug resistance: a comprehensive review. Nano Today. 2013;8(3):313–31.
42. Zhao YZ, Dai DD, Lu CT, Chen LJ, Lin M, Shen XT, et al. Epirubicin loaded with propylene glycol liposomes significantly overcomes multidrug resistance in breast cancer. Cancer Lett. 2013;330(1):74–83.
43. Wang X, Rao Z, Qin H, Zhang G, Ma Y, Jin Y, et al. Effect of hesperidin on the pharmacokinetics of CPT-11 and its active metabolite SN-38 by regulating hepatic Mrp2 in rats. Biopharm Drug Dispos. 2016;37(7):421–32.
44. Patel HM, Moghimi SM. Serum-mediated recognition of liposomes by phagocytic cells of the reticuloendothelial system - The concept of tissue specificity. Adv Drug Deliv Rev. 1998;32(1-2):45–60.
45. Patel HM. Serum opsonins and liposomes: their interaction and opsonophagocytosis. Crit Rev Ther Drug Carrier Syst. 1992;9(1):39–90.
46. Gabizon A, Catane R, Uziely B, Kaufman B, Safra T, Cohen R, et al. Prolonged circulation time and enhanced accumulation in malignant exudates of doxorubicin encapsulated in polyethyleneglycol coated liposomes. Cancer Res. 1994;54(4):987–92.
47. Bayever E, Fitzgerald JB, Kim J, Klinz S. Treatment of breast cancer with liposomal irinotecan. Google Patents; 2016.
48. Adkins CE, Mohammad AS, Terrell-Hall TB, Dolan EL, Shah N, Sechrest E, et al. Characterization of passive permeability at the blood-tumor barrier in five preclinical models of brain metastases of breast cancer. Clin Exp Metastasis. 2016;33(4):373–83.
49. Liu D, Yang P, Hu D, Liu F. Minocycline hydrochloride liposome controlled-release gel improves rat experimental periodontitis. Hua xi kou qiang yi xue za zhi = Huaxi kouqiang yixue zazhi = West China Journal of Stomatology. 2013;31(6):592–6.
50. Ostrowski AD, Lin BF, Tirrell MV, Ford PC. Liposome encapsulation of a photochemical NO precursor for controlled nitric oxide release and simultaneous fluorescence imaging. Mol Pharm. 2012;9(10):2950–5.
51. Lin NU, Bellon JR, Winer EP. CNS metastases in breast cancer. J Clin Oncol Off J Am Soc Clin Oncol. 2004;22(17):3608–17.
52. Boogerd W, Dalesio O, Bais EM, van der Sande JJ. Response of brain metastases from breast cancer to systemic chemotherapy. Cancer. 1992;69(4):972–80.